

Frustrated Lewis Pairs

Divergent CO₂ Activation by Tuning the Lewis Acid in Iron-Based Bimetallic Systems

Helena Corona⁺, Marina Pérez-Jiménez⁺, Felipe de la Cruz-Martínez, Israel Fernández,* and Jesús Campos*

Abstract: Bimetallic motifs mediate the selective activation and functionalization of CO₂ in metalloenzymes and some recent synthetic systems. In this work, we build on the nascent concept of bimetallic frustrated Lewis pairs (FLPs) to investigate the activation and reduction of CO₂. Using the Fe⁰ fragment [(depe)₂Fe] (depe = 1,2-bis(diethylphosphino)ethane) as base, we modify the nature of the partner Lewis acid to accomplish a divergent and highly chemoselective reactivity towards CO₂. [Au(PMe₂Ar)]⁺ irreversibly dissociates CO₂, Zn(C₆F₅)₂ and B(C₆F₅)₃ yield different CO₂ adducts stabilized by push-pull interactions, while Al(C₆F₅)₃ leads to a rare heterobimetallic C–O bond cleavage, and thus to contrasting reduced products after exposure to dihydrogen. Computational investigations provide a rationale for the divergent reactivity, while Energy Decomposition Analysis-Natural Orbital for Chemical Valence (EDA-NOCV) method substantiates the heterobimetallic bonding situation.

Introduction

The selective transformation of CO₂ into reduced C₁ products is one of the most challenging and environmentally

appealing reactions pursued by chemists in the last decades.^[1] Inspiring designing principles come out from nature, where CO-dehydrogenase (CODH) enzymes mediate the redox interconversion between CO₂ and CO. Crucial for their efficiency are their Ni/Fe and Mo/Cu bimetallic active sites,^[2] capable of cooperatively activating carbon dioxide by means of complementary Lewis acidic/Lewis basic behaviour of the two metals. Not surprisingly, artificial bioinspired approaches that rely on this type of bimetallic synergism have attracted great attention in recent times.^[3,4] In a similar vein, Frustrated Lewis pairs (FLPs) operate upon analogous premises for the activation of CO₂,^[5] including metal-containing FLP-type structures^[6] that resemble as well the active site of CODH enzymes.^[7] It has also been well recognized that Lewis acidic metals drastically influence the capacity of redox active sites to reduce CO₂,^[8] either by serving as Z-type ligands^[9] or by directly contributing to stabilize key intermediates during CO₂ reduction.^[10]

Regardless of the precise mode of action, the use of bimetallic combinations based on non-precious metals to reduce CO₂ remains an important challenge. Mankad and co-workers have very recently described a heterobimetallic complex based on the two most abundant metals in the Earth crust, iron and aluminium, which activate CO₂ via radical intermediates.^[11] The use of aluminium has indeed shown success in other bimetallic combinations, both with transition^[12] and main group^[13] metals. In fact, a recent study by Camp et al. evidenced the cleavage of a C–O bond of CO₂ by induced umpolung reactivity at an Ir/Al system.^[14] Reverse polarity has been exploited by Aldridge and Goicoechea for group 11-alumanyl bimetallic complexes in CO₂ activation^[15] (Figure 1a). Inspired by these results and building on our prior studies on bimetallic FLPs,^[16] we decided to investigate the cooperative activation of CO₂ using the synthon [(depe)₂Fe] (depe = 1,2-bis(diethylphosphino)ethane) as a Fe⁰ metallic base. We report divergent CO₂ reactivity resulting from varying the nature of the partner Lewis acid. This spans from CO₂ dissociation in the case of gold to different modes of bimetallic activation for fluorinated zinc and borane Lewis acids and even C–O bond cleavage in the case of the highly electrophilic Al(C₆F₅)₃ (Figure 1b).

Results and Discussion

We decided to use the Fe⁰ fragment [(depe)₂Fe] as a metallic Lewis base because its corresponding CO₂ adduct (**1**) is

[*] H. Corona,⁺ Dr. M. Pérez-Jiménez,⁺ Dr. F. de la Cruz-Martínez, Dr. J. Campos
 Instituto de Investigaciones Químicas (IIQ), Departamento de Química Inorgánica and Centro de Innovación en Química Avanzada (ORFEO—CINQA), Universidad de Sevilla and Consejo Superior de Investigaciones Científicas (CSIC)
 Avenida Américo Vespucio 49, 41092 Sevilla (Spain)
 E-mail: jesus.campos@iiq.csic.es

Dr. I. Fernández
 Departamento de Química Orgánica I and Centro de Innovación en Química Avanzada (ORFEO—CINQA), Facultad de Ciencias Químicas, Universidad Complutense de Madrid
 28040 Madrid (Spain)
 E-mail: israel@quim.ucm.es

[†] These authors contributed equally to this work.

© 2022 The Authors. Angewandte Chemie International Edition published by Wiley-VCH GmbH. This is an open access article under the terms of the Creative Commons Attribution Non-Commercial NoDerivs License, which permits use and distribution in any medium, provided the original work is properly cited, the use is non-commercial and no modifications or adaptations are made.

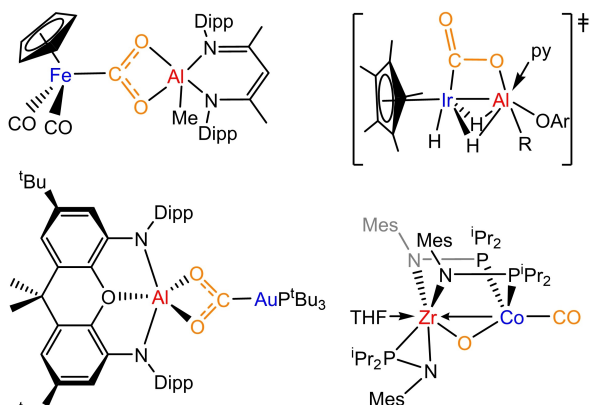
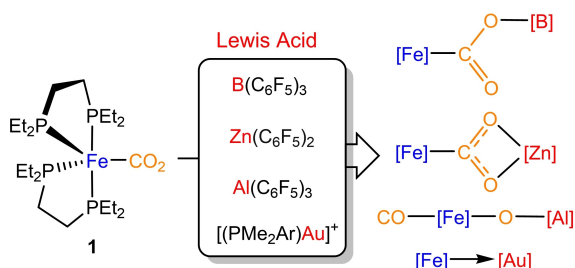
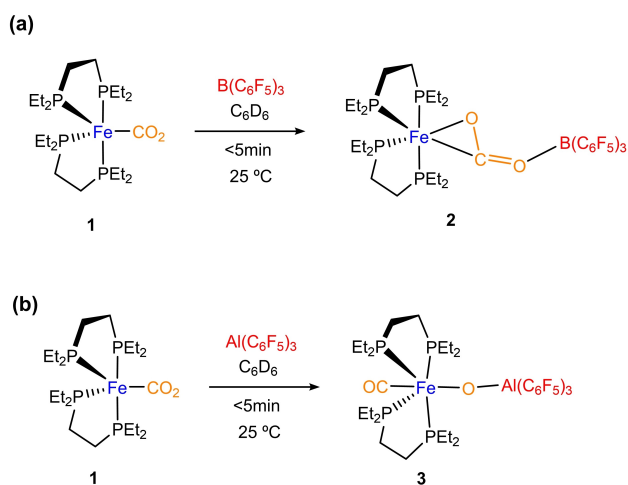
(a) Representative examples of bimetallic CO₂ activation(b) This work: divergent bimetallic CO₂ activation

Figure 1. a) Representative examples of bimetallic CO₂ activation pathways relevant to the present work; b) divergent bimetallic CO₂ activation routes as a function of the Lewis acid (this work).

readily accessible^[17a] and exhibits a rich carbon dioxide functionalization chemistry.^[17b,c] Besides, Szymczak and co-workers used the latter to investigate the activation of dinitrogen by push-pull interactions.^[18] In line with that work, we started our investigations by treating complex [(depe)₂Fe(CO)₂] (**1**) with the acidic borane B(C₆F₅)₃ (Scheme 1a). The addition of the borane to toluene or



Scheme 1. Activation of CO₂ by treating Fe–CO₂ adduct **1** with Lewis acids B(C₆F₅)₃ (a) and Al(C₆F₅)₃ (b).

benzene solutions of **1** promotes an immediate change in colour from orange to pink solutions due to the formation of complex **2**, which could be isolated in 82 % yield after the workup.

Monitoring the reaction by ³¹P{¹H} NMR we observed the complete consumption of the starting iron species (87.0, 79.0, 70.0 and 62.6 ppm) and the appearance of a new set of three broad signals (85.1, 80.4 and 70.4 ppm, with relative intensities 1:1:2 in benzene-*d*₆). The corresponding ¹¹B-¹H NMR spectrum exhibited a broad signal at –1.6 ppm similar to the chemical shift observed for the somewhat related [(depe)₂Fe(N₂)B(C₆F₅)₃] product (–6.3 ppm) from N₂-activation.^[18] IR spectroscopy provided relevant information, as two stretch bands were found at 1641 cm^{–1} and 1251 cm^{–1} indicative of a CO₂ unit.^[7,8] Moreover, a ¹³C-¹H NMR signal at 214.8 ppm in thf-*d*₈ evidences that a carbonyl group is still retained in complex **2**.^[19]

We were able to confirm its structure as the binuclear product [(depe)₂Fe(μ-CO₂)B(C₆F₅)₃] (**2**) (Figure 2a), in

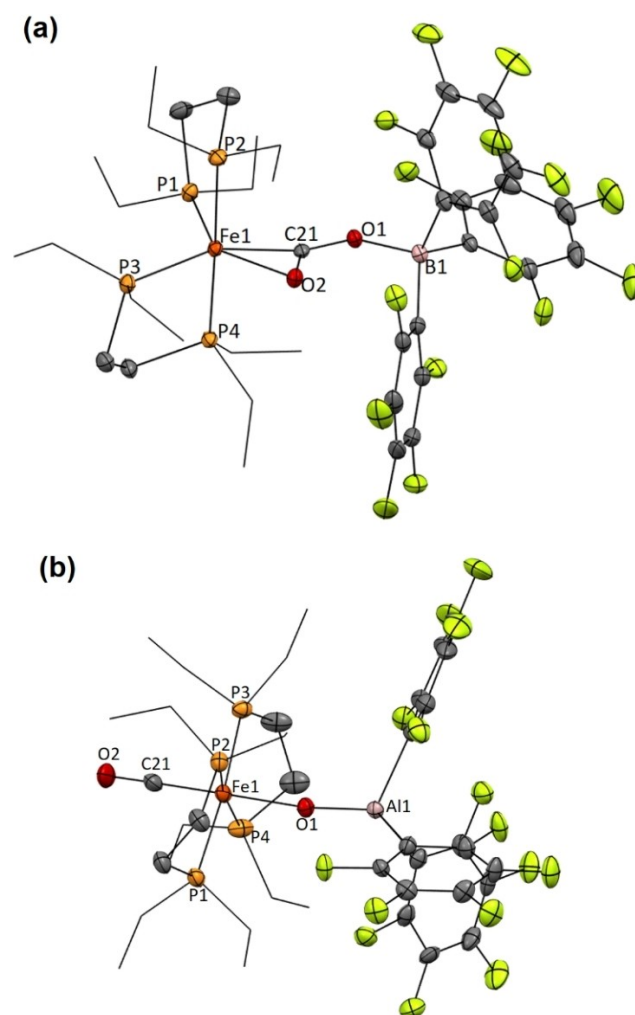


Figure 2. ORTEP diagrams for complexes **2** (a) and **3** (b). Hydrogen atoms have been excluded, and ethyl groups of depe ligand are represented in wire-frame format for clarity. Thermal ellipsoids are set at 50% probability.

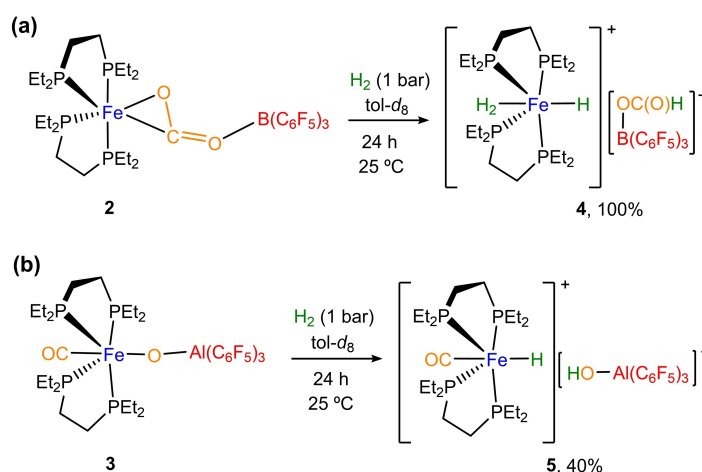
which the activated CO_2 bridges the Fe/B pair in a $\mu\text{-CO}_2\text{-1}\kappa\text{O}^1\text{:C}^1\text{:2}\kappa\text{O}^2$ fashion. The molecular structure is comparable to the other four crystallized bridging CO_2 -adducts stabilized by push-pull interactions between a basic metal (Ni, Pt, Mo and Re) and a borane.^[6a,b,8] η^2 -Coordination to iron is evidenced by the corresponding Fe1–O2 (2.212(2) Å) and Fe1–C21 (1.861(3) Å) bond lengths. The other oxygen atom is linked to the borane with an O1–B1 bond length of 1.531(5) Å. The O2–C21–O1 angle of 126.61(3)° is practically identical to that one found for precursor **1** (124(2)°) (Figure 2a).^[17] Nonetheless, the presence of the borane results in the elongation of the connected C21–O1 bond (1.305(4) Å) compared to the one bound to iron (C21–O2, 1.249(3) Å), being also the former C21–O1 bond longer than in adduct **1** (1.25(3) and 1.28(2) Å).

Increasing the acidity of the Lewis acid partner by treating **1** with the analogous $\text{Al}(\text{C}_6\text{F}_5)_3$,^[20] likewise resulted in an immediate reaction leading to a yellow solution in benzene- d_6 . However, the first hint pointing to a contrasting reactivity arose from $^{31}\text{P}\{^1\text{H}\}$ NMR analysis, where a single signal was recorded at 67.9 ppm. At variance with compound **2**, this suggests the formation of a new compound (**3**) with high symmetry (Scheme 1b). Moreover, its corresponding IR spectrum presents an intense band at 1914 cm^{-1} , characteristic of a CO moiety. Crystals suitable for X-ray diffraction studies were grown by placing a concentrated toluene solution of **3** in the glovebox freezer at -30°C for one day (27% yield), revealing the bimetallic cleavage of a C–O bond to yield $[(\text{depe})_2(\text{CO})\text{Fe}(\mu\text{-O})\text{Al}(\text{C}_6\text{F}_5)_3]$ (Figure 2b). The $^{13}\text{C}\{^1\text{H}\}$ NMR experiment of complex **3** (in thf-d_8) features a signal at 213.6 ppm which further confirms the presence of a CO ligand.^[19] For comparison, we performed the analogous reaction using AlEt_3 as the electrophilic fragment. Although the resulting product could not be isolated, we were able to record a $^{31}\text{P}\{^1\text{H}\}$ NMR spectrum (Figure S13) which exhibited the same pattern and multiplicity as complex **2**, suggesting the formation of a similar CO_2 -adduct and pointing out to the need of the perfluori-

nated substituents to accomplish the cleavage the C–O bond.

The formation of **3** constitutes a highly unusual event from different standpoints. First, while examples of bimetallic CO_2 activation have grown in number in the last decade,^[3] those in which the cleavage of a C–O bond is achieved are more limited.^[21] In like manner, heterobimetallic versions are even scarcer.^[22,14] Structurally, compound **3** represents the first example of an oxo-bridged Fe/Al complex, which is of interest considering the limited accessibility but high reactivity of oxo-bridged heterobimetallic motifs, for instance in the context of C–H bond functionalization.^[23] The Fe1–O1–Al1 angle is almost linear (171.9(4)°), while the O1–Al1 and Fe1–O1 bonds feature distances of 1.685(7) and 2.007(7) Å, respectively. Note that the latter is larger than those reported for oxo-bridged diiron complexes,^[24] probably as a result of the interaction with the highly acidic and crowded alane fragment. The Fe(CO) group presents the characteristic structural data for an iron carbonyl fragment^[25] and is in *trans* position to the Fe–($\mu\text{-O}$)Al bond.

We next wondered whether the contrasting reactivity of Fe/B vs Fe/Al pairs would result in dissimilar reduction pathways for CO_2 . Firstly, it is important to remark that the reaction of **1** with dihydrogen leads to the quantitative formation of the previously described Fe^{II} dihydride species $[(\text{depe})_2\text{Fe}(\text{H})_2]$,^[26] a result that is in stark contrast to the reaction outcomes in the presence of both borane and alane. Thus, exposure of **2** to dihydrogen under mild conditions (1 bar, 25°C) resulted in the formal hydrogenation of the Fe–C bond towards compound **4** in a quantitative manner (Scheme 2a). This ion pair exhibits distinctive resonances at 92.3 ppm and -3.0 ppm in the $^{31}\text{P}\{^1\text{H}\}$ and $^{11}\text{B}\{^1\text{H}\}$ NMR spectra, respectively. Besides, a characteristic ^1H NMR signal at 8.6 ppm due to the formate and two low-frequency signals at -11.0 and -15.1 ppm due to the dihydrogen and hydride ligands respectively, which match prior data for the individual fragments of **4**,^[27] further confirm its formulation (Figures S14–S16). In accordance, its IR spectrum reveals a



Scheme 2. Reactivity of compounds **3** and **4** with H_2 . Spectroscopic yields were measured by $^{31}\text{P}\{^1\text{H}\}$ NMR using triphenyl phosphine oxide as internal standard.

band at 1643 cm^{-1} assigned to the $\nu(\text{C}=\text{O})$ stretching vibration (Figure S17).^[28,27c]

Interestingly, when complex **3** is exposed to dihydrogen atmosphere under the same reaction conditions, the oxo $\text{Fe}(\mu\text{-O})\text{Al}$ bridge is broken resulting in the appearance of a new Fe-H fragment inferred from a distinctive low-frequency signal in the ^1H NMR spectrum at -14.7 ppm (br). This hydride ligand belongs to a new major species (**5**) that is formed in around 40% spectroscopic yield and resonates in the $^{31}\text{P}\{^1\text{H}\}$ NMR spectrum at 65.4 ppm (Figures S18–S19). IR spectroscopy of the reaction mixture revealed two bands at 1902 and 3396 cm^{-1} (Figure S20). While we attribute the former to the corresponding CO ligand of **5**, the latter broad band accounts for the formation of a new OH bond. We attribute the moderate yield measured for compound **5**, at least in part, to its poor solubility in toluene. In fact, performing the reaction in a more polar solvent such as CD_2Cl_2 , we could achieve full conversion of **3** and formation of **5** in better yields (ca. 75%), although accompanied by the appearance of other minor unidentified species (Figure S21). These results are in agreement with the hydrogenolysis of the Fe-O bond in **3** to yield compound **5** (Scheme 2b), once more matching the spectroscopic data available for related ion pairs based on the $[(\text{depe})_2\text{Fe}(\text{H})(\text{CO})]^+$ cation.^[29] Overall, this sequential transformation is reminiscent of that mediated by CODH enzymes, where bimetallic CO_2 activation is followed by reduction with an electron transfer reagent, dihydrogen in the present case.

The complete selectivity towards either CO_2 activation or C–O bond cleavage resulting from an apparently

innocent modification of the Lewis acidic site prompted us to investigate the bimetallic mechanism in more detail. To this end, Density Functional Theory (DFT) calculations were carried out at the dispersion corrected PCM(toluene)-BP86-D3/def2-TZVPP//BP86-D3/def2-SVP level. Figure 3 shows the computed reaction profiles for the reactions of $[(\text{depe})_2\text{Fe}(\text{CO}_2)]$ (**1**) with $\text{B}(\text{C}_6\text{F}_5)_3$ and $\text{Al}(\text{C}_6\text{F}_5)_3$.

In both cases, the reaction begins with the highly exergonic formation of the dative bond between the lone-pair of the $\text{O}(\text{=C})$ moiety of **1** and the vacant p atomic orbital of the group 13 atom of the Lewis acid leading to the observed species **2** and the analogous complex **2-Al**. Although both processes are highly exergonic, the higher Lewis acidity of $\text{Al}(\text{C}_6\text{F}_5)_3$ becomes evident from the much higher exergonicity computed for the formation of **2-Al** ($\Delta G_{\text{R}} = -46.6\text{ kcal mol}^{-1}$ vs $-23.0\text{ kcal mol}^{-1}$). Species **2-Al** is then transformed into **INT1** through **TS1**, a saddle point associated with the slippage of the bridging CO_2 ligand with a feasible activation barrier of $17.7\text{ kcal mol}^{-1}$ in a slightly endergonic transformation ($\Delta G_{\text{R}} = 7.4\text{ kcal mol}^{-1}$). Intermediate **INT1** evolves to **INT2** via **TS2**, which is associated with the rupture of the OC-O bond. This crucial step requires a low barrier of only 9.1 kcal mol^{-1} and is again slightly endergonic ($\Delta G_{\text{R}} = 2.9\text{ kcal mol}^{-1}$). The transformation ends up with the isomerization of **INT2**, where the carbonyl ligand is placed *cis* to the O-Al moiety, into the corresponding *trans*-**3** complex. This final step is highly exergonic ($\Delta G_{\text{R}} = -16.6\text{ kcal mol}^{-1}$) and compensates the previous endergonic steps therefore driving the complete transformation forward towards the formation of the observed complex **3**. A similar reaction profile was com-

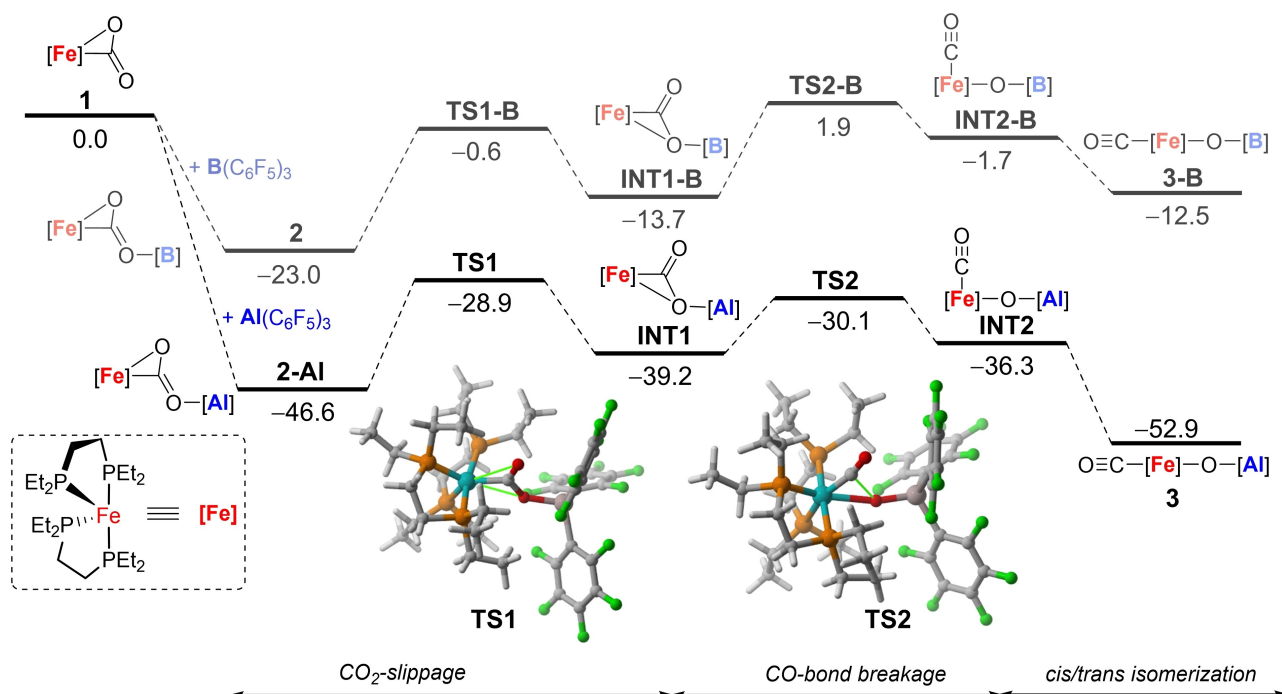
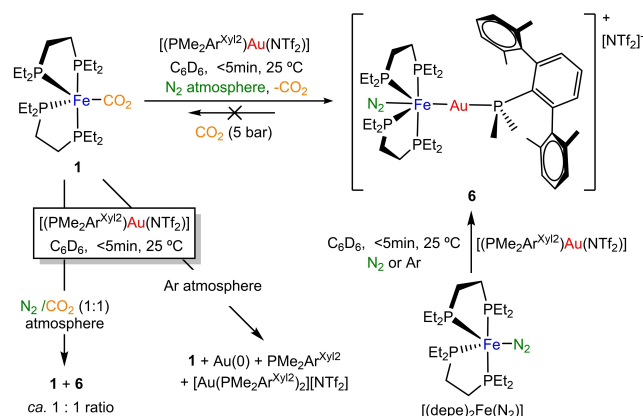


Figure 3. Computed reaction profiles for the reactions of $[(\text{depe})_2\text{Fe}(\text{CO}_2)]$ (**1**) with $\text{B}(\text{C}_6\text{F}_5)_3$ and $\text{Al}(\text{C}_6\text{F}_5)_3$. Relative free energies (ΔG , at 298 K) are given in kcal mol^{-1} . All data have been computed at the PCM(toluene)-BP86-D3/def2-TZVPP//BP86-D3/def2-SVP level.

puted for the boron counterpart **2**, but at variance, the formation of the related species **3-B** is thermodynamically not favoured. Despite the computed barriers involving **TS1-B** and **TS2-B** are again feasible at room temperature ($\Delta G^\ddagger = 22.4$ and 15.6 kcal mol⁻¹, respectively), a similar thermodynamic driving force to that commented above for the profile involving Al(C₆F₅)₃ is lacking for the process involving B(C₆F₅)₃ and for this reason, the experimentally observed complex **2** remains the global minimum on the potential energy surface. The transient formation of **2-AI** could be substantiated by monitoring the reaction between **1** and Al(C₆F₅)₃ at -80°C , which starts with the formation of a new species characterized by ³¹P{¹H} NMR resonances at 87.2, 80.3, 74.1 and 70.0 ppm that cleanly evolves to compound **3** upon mild warm-up.

The above divergent reactivity encouraged us to examine the role of other metallic Lewis acids to be combined with CO₂-adduct **1**. We first investigated the addition of the highly electrophilic Au^I compound [(PMe₂Ar^{Xyl2})Au(NTf₂)],^[30] where Ar^{Xyl2} stands for C₆H₃-2,6-(C₆H₃-2',6'-(CH₃)₂)₂ and NTf₂ for [N(SO₂CF₃)₂]⁻. This Au^I species has been exploited in our group for the design of bimetallic FLPs,^[16] since it contains a sterically shielding terphenyl phosphine and a weakly-coordinating triflimdate ligand that facilitates access to the aimed electrophilic [(PMe₂Ar^{Xyl2})Au]⁺ moiety. Treating **1** with an equimolar amount of [(PMe₂Ar^{Xyl2})Au(NTf₂)] under nitrogen atmosphere (Scheme 3) resulted in dissociation of the CO₂ ligand and formation of an Fe⁰→Au^I metal-only Lewis pair (**6**).^[31] In fact, the same compound can be easily prepared by adding [(PMe₂Ar^{Xyl2})Au(NTf₂)] to the nitrogen adduct [(depe)₂Fe(N₂)].

Interestingly, the former reaction entails an irreversible ligand substitution defined by the coordination of a N₂ molecule from the reaction atmosphere, in a *trans* position towards the Fe–Au bond. It is important to remark that substitution of CO₂ by the very weakly coordinating N₂ ligand is rare^[7] and, for this system, it has only been observed in the presence of gold, further certifying the crucial influence exerted by coordination of Lewis acids to



Scheme 3. Reactivity of **1** with gold complex [(PMe₂Ar^{Xyl2})Au(NTf₂)] as a function of the atmosphere.

transition metals. Formation of **6** from either [(depe)₂Fe(CO₂)] or [(depe)₂Fe(N₂)] contrasts with prior studies from Simonneau where Au^I compounds are prone to participate in push-pull interactions to activate dinitrogen,^[32] while herein the formation of the Fe⁰→Au^I dative bond prevails. Changing the atmosphere to an approximate equimolar N₂/CO₂ mixture led to the presence of both precursor **1** and bimetallic adduct **6**, along with other decomposition products. In contrast, under argon atmosphere we could only observe decomposition of the gold complex, forming a black solid precipitate, free terphenyl phosphine and [Au(PMe₂Ar^{Xyl2})₂][NTf₂], as detected by ³¹P{¹H} NMR monitoring experiments, which evinces the surprisingly important stabilizing role played by the dinitrogen ligand. Nonetheless, complex **6** is thermally unstable and decomposes to metallic gold and free phosphine after minutes in benzene or toluene solutions. Attempts to prepare analogous species with bulkier phosphine ligands (PMe₂Ar^{Dipp2} or PCyp₂Ar^{Xyl2}) directly led to decomposition products.

Despite its reduced stability, we managed to characterize compound **6** by spectroscopic means (¹H, ³¹P NMR and IR spectroscopy) and authenticate its molecular structure by X-ray diffraction studies (Figure 4). It exhibits two characteristic signals in the ³¹P{¹H} NMR spectrum, a doublet at 72.4 ppm (³J_{PP} = 42 Hz) and a quintet at 31.0 ppm (³J_{PP} = 42 Hz). The N≡N bond of the coordinated dinitrogen is slightly shorter (1.12(2) Å) than in its monometallic parent species [(depe)₂Fe(N₂)] (1.139(13) Å),^[33] which we attribute to reduced donation from Fe⁰ to a π*(NN) orbital as a result of the competing donation from iron to gold (see below). In fact, the Fe–N bond in **6** is elongated to 1.83(1) Å compared to 1.748(8) Å in [(depe)₂Fe(N₂)], while the formation of a dative Fe→Au bond is characterized by a distance of 2.530(2) Å (Figure 4). All these metrics are in accordance with an IR stretching band for N₂ in complex **6** sharply shifted to 2057 cm⁻¹ with respect to 1955 cm⁻¹ found for [(depe)₂Fe(N₂)].^[33]

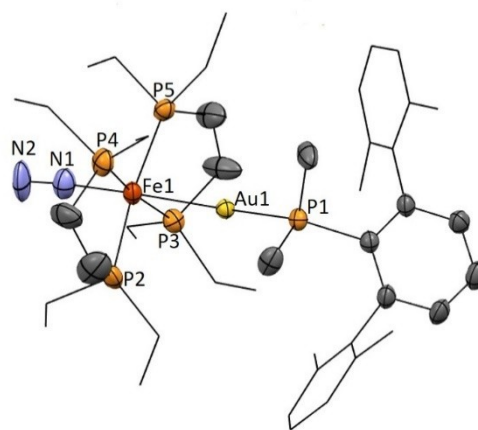


Figure 4. ORTEP diagram for complex **6**⁺. Hydrogen atoms have been excluded, and ethyl groups of depe ligand and flanking aryl rings of the terphenyl phosphine are represented in wire-frame format for clarity. Thermal ellipsoids are set at 50% probability.

The particular bonding situation of the newly prepared complex **6** in comparison with the parent species $[(\text{depe})_2\text{Fe}(\text{N}_2)]$ deserves further analysis. With the help of the Energy Decomposition Analysis-Natural Orbital for Chemical Valence (EDA-NOCV) method, we first compared the nature of the Fe-N₂ bond in $[(\text{depe})_2\text{Fe}(\text{N}_2)]$ and the bimetallic cation $[(\text{N}_2)(\text{depe})_2\text{Fe}-\text{Au}(\text{PMe}_2\text{Ar}^{\text{Xyl}2})]^+$ (**6**⁺) at the relativistic and dispersion corrected ZORA-BP86-D3/TZ2P//BP86-D3/def2-SVP level. Our calculations indicate that the presence of the gold(I) fragment makes the Fe-N₂ bond weaker as confirmed by the computed lower interaction energy in **6**⁺ (see Table S1 in the Supporting Information). The partitioning of the ΔE_{int} term indicates that the strength of the orbital and electrostatic interactions is comparable being the former slightly stronger in both species. Interestingly, three different orbital interactions dominate the total ΔE_{orb} term, namely the σ -donation from the N₂ to the transition metal fragment (denoted as $\Delta E(\rho_1)$) and two π -backdonations from the transition metal into both π^* molecular orbitals of the N \equiv N ligand (denoted as $\Delta E(\rho_2)$ and $\Delta E(\rho_3)$, respectively, Figure 5). From the data in Table S1 and Figure 5, it becomes evident that the out-of-plane π -backdonation (ρ_2) is significantly weaker ($\Delta\Delta E(\rho_2) = 20 \text{ kcal mol}^{-1}$) in the cationic complex **6**⁺ as a result of the reduced electronic density at the Fe⁰ centre by coordination to the Au^I fragment. As a consequence, the N \equiv N bond is stronger in **6** which is reflected in the observed higher IR stretching and shorter distance. Finally, we also analyzed the Fe-Au bond in **6**⁺ with the EDA-NOCV method. Although the Fe-Au interaction is mainly electrostatic (the ΔE_{elstat}

term contributes ca. 56 % to the total ΔE_{int}), our calculations confirm the dative nature of the Fe⁰→Au^I bond (associated $\Delta E(\rho) = -68.4 \text{ kcal mol}^{-1}$, see Table S1) involving the donation from a doubly-occupied d atomic orbital of Fe⁰ to the vacant s atomic orbital of Au^I.^[34]

As aforementioned, we were intrigued by the ability of gold to promote irreversible ligand substitution between CO₂ and N₂. Although exposure of **6** to CO₂ under more forcing pressure conditions (5 bar) did not offer any hint of CO₂ coordination (Scheme 3), the addition of one equivalent of B(C₆F₅)₃ under CO₂ atmosphere (0.5 bar) immediately generates complex **2**. Our calculations are in line with this observation as the highly endergonic reaction **6**⁺ + CO₂ → **1** + AuNTf₂ + N₂ ($\Delta G_{\text{R}} = +14.6 \text{ kcal mol}^{-1}$) becomes exergonic in the presence of B(C₆F₅)₃ to produce **2** ($\Delta G_{\text{R}} = -8.4 \text{ kcal mol}^{-1}$). This behaviour contrasts with the ability of the gold complex to displace the borane in $[(\text{depe})_2\text{Fe}(\text{N}_2)\text{B}(\text{C}_6\text{F}_5)_3]$, which readily occurs to form complex **6** upon mixing the two species. Analogously, we have proved the inertness of the Fe/Au bimetallic compound **6** towards B(C₆F₅)₃ in the absence of carbon dioxide, which according to our calculations is indeed a highly endergonic (thus, unfeasible) process ($\Delta G_{\text{R}} = +43.8 \text{ kcal mol}^{-1}$). These results suggest that the most thermodynamically stable compound of the series is compound **2**.

To complete these studies, we finally examined the use of Zn(C₆F₅)₂ as a Lewis acid, owing to its higher oxophilicity compared to gold^[35] and thus a presumed enhanced ability to activate CO₂. In fact, treating a thf solution of precursor **1** with Zn(C₆F₅)₂ in equimolar amounts resulted in a rapid

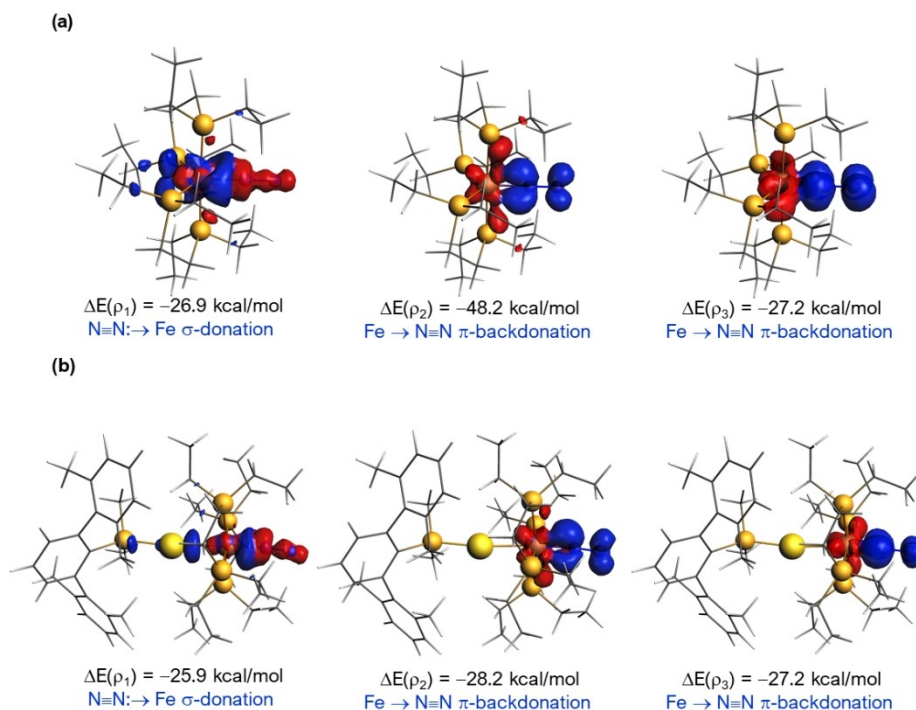


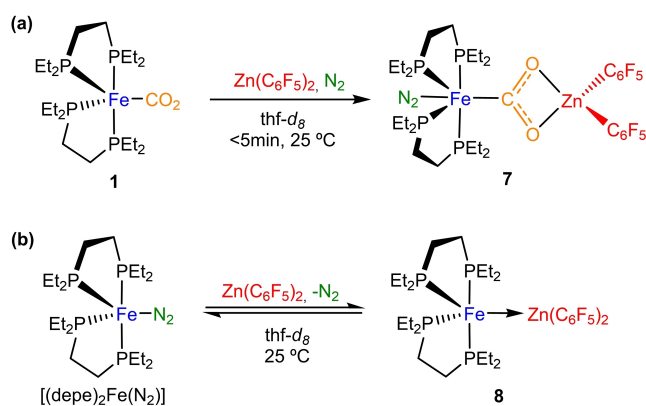
Figure 5. Contour plots of NOCV deformation densities $\Delta\rho$ and associated energies $\Delta E(\rho)$ (computed at the ZORA-BP86-D3/TZ2P//BP86-D3/def2-SVP level) in $[(\text{depe})_2\text{Fe}(\text{N}_2)]$ (a) and **6**⁺ (b). Electron-density charge flows in the direction red→blue.

colour change from orange to pink. The formation of a new compound **7** (Scheme 4a) is evidenced by $^{31}\text{P}\{^1\text{H}\}$ NMR, where a broad signal at 77.8 ppm was recorded in thf-d_8 at 25 °C. This signal becomes a set of four broad multiplets (89.1, 80.9, 74.7 and 67.9 ppm) when the temperature was decreased to -20 °C. Single-crystals suitable for X-ray diffraction analysis were grown from a concentrated toluene solution at -30 °C (35 % yield), unveiling the anticipated activation of CO_2 in a bimetallic manner (Figure 6). At variance with $\text{B}(\text{C}_6\text{F}_5)_3$, the CO_2 molecule now bridges the two metals in a $\mu\text{-CO}_2\text{-}1\kappa\text{C}^1:2\kappa\text{O}^1:\text{O}^2$ fashion. The corresponding structural parameters are comparable to previous examples that exhibit this type of binding.^[4,12,13c] η^2 -coordination to zinc forces the O–C–O angle to diminish to 114(2)° (c.f. 124(2)° in **1**). Activation of CO_2 upon zinc coordination is also discernible by a slight elongation of the C–O bonds to an average value of 1.29 Å (1.27(2) for O1–C21 and 1.31(2) Å for O2–C21 distances) compared to the average value of 1.26 Å in complex **1** (1.28(2) and 1.25(3) Å values for the two C–O distances).^[17] Intriguingly, a molecule of N_2

coordinates to the Fe^0 centre upon CO_2 activation to yield a highly unusual structure, namely the first organometallic species structurally characterized in which both N_2 and CO_2 , typically very poorly coordinating ligands, are bound to the same metal. Their presence is in accordance with its corresponding IR spectrum, where bands at 1633 and 2105 cm^{-1} are assigned to CO_2 and N_2 , respectively. The function of the iron centre as a Lewis base for the activation of CO_2 results in a reduced $\text{N}\equiv\text{N}$ bond length of 1.07(2) Å, even shorter than in compound **6** (1.12(2) Å).

The unexpected coordination of dinitrogen in **7** led us to examine the reactivity of $[(\text{depe})_2\text{Fe}(\text{N}_2)]$ with $\text{Zn}(\text{C}_6\text{F}_5)_2$ (Scheme 4b). Conversely, in the absence of CO_2 , the metal only Lewis adduct **8** characterized by a dative $\text{Fe}^0\text{-Zn}^{\text{II}}$ bond ($d_{\text{FeZn}}=2.561$ Å; see Figure S36) is produced as the major species, with concomitant release of dinitrogen. Nonetheless, complex **8** exhibits a dynamic equilibrium in solution with its separated fragments, being the Fe–Zn bond cleavage favoured at low temperatures (see Supporting Information). In fact, compound **8** could be isolated as green crystals at -30 °C in 28 % yield. The lability of the bimetallic bond is also confirmed by the addition of one equivalent of $\text{B}(\text{C}_6\text{F}_5)_3$ under CO_2 atmosphere, which results in quantitative formation of **2**. However, exposure of **8** to CO_2 (1 atm) results in the formation of unidentified products and phosphine ligand dissociation.

Comparing the C–Zn–C angle of both zinc-based structures, it diminishes from 135.6(7)° in **7** to 100.2(1)° in **8**, significantly reduced compared to other transition metal base-zinc Lewis adducts.^[36] Once more, this result contrasts with the push-pull activation of N_2 observed before for the same iron fragment in the presence of $\text{B}(\text{C}_6\text{F}_5)_3$ ^[18] and attests the importance of tuning the nature of Lewis acids in bimetallic architectures as a crucial designing principle for bond activation studies.



Scheme 4. Reactivity of Fe^0 compounds with $\text{Zn}(\text{C}_6\text{F}_5)_2$.

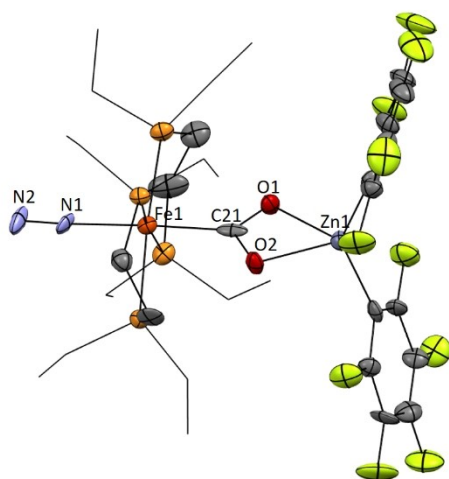


Figure 6. ORTEP of complex **7**. Hydrogen atoms have been excluded, and ethyl groups of depe ligand are represented in wire-frame format for clarity. Thermal ellipsoids are set at 50% probability.^[37]

Conclusion

We have demonstrated that the choice of Lewis acid for the binuclear activation of carbon dioxide through push-pull forces is of paramount importance to modulate reaction selectivity. In fact, maintaining a common Lewis basic Fe^0 synthon ($[(\text{depe})_2\text{Fe}(\text{CO}_2)]$), we disclose a completely divergent reactivity that span from irreversible CO_2 dissociation, to its activation by two dissimilar modes and up to the rare bimetallic cleavage of one of the C–O bonds. We have performed computational studies that provide solid understanding on the observed divergent reactivity and substantiate the bonding scenario by means of state-of-the-art methods. Overall, the results of this work offer fundamental knowledge on the way to developing bimetallic efficient strategies for the valorisation of carbon dioxide.

Acknowledgements

This work was supported by the European Research Council (ERC Starting Grant, CoopCat, Project 756575), Spanish

MCIN/AEI/10.13039/501100011033 (Projects PID2019-110856GA-I00, PID2019-106184GB-I00 and RED2018-102387-T) and Junta de Andalucía (P18-FR-4688). F. de la C.-M. acknowledges the Spanish Ministry of Universities for a Margarita Salas postdoctoral fellowship.

Conflict of Interest

The authors declare no conflict of interest.

Data Availability Statement

The data that support the findings of this study are available in the supplementary material of this article.

Keywords: Bimetallic · CO₂ Activation · Cooperativity · Lewis Acids · Push-Pull Interactions

- [1] a) M. D. Burkart, N. Hazari, C. L. Tway, E. L. Zeitler, *ACS Catal.* **2019**, *9*, 7937–7956; b) A. M. Appel, J. E. Bercaw, A. B. Bocarsly, H. Dobbek, D. L. DuBois, M. Dupuis, J. G. Ferry, E. Fujita, R. Hille, P. J. A. Kenis, C. A. Kerfeld, R. H. Morris, C. H. F. Peden, A. R. Portis, S. W. Ragsdale, T. B. Rauchfuss, J. N. H. Reek, L. C. Seefeldt, R. K. Thauer, G. L. Waldrop, *Chem. Rev.* **2013**, *113*, 6621–6658.
- [2] a) J.-H. Jeoung, H. Dobbek, *Science* **2007**, *318*, 1461–1464; b) H. Dobbek, L. Gremer, R. Kiefersauer, R. Huber, O. Meyer, *Proc. Natl. Acad. Sci. USA* **2002**, *99*, 15971–15976; c) M. E. Ahmed, S. Adam, D. Saha, J. Fize, V. Artero, A. Dey, C. Duboc, *ACS Energy Lett.* **2020**, *5*, 3837–3842; d) A. Mouchfiq, T. K. Todorova, S. Dey, M. Fontecave, V. Mougel, *Chem. Sci.* **2020**, *11*, 5503–5510; e) Y. Li, M. Gomez-Mingot, T. Fogeron, M. Fontecave, *Acc. Chem. Res.* **2021**, *54*, 4250–4261.
- [3] a) N. P. Mankad, *Trends Chem.* **2021**, *3*, 159–160; b) S. Sinhababu, Y. Lakliang, N. P. Mankad, *Dalton Trans.* **2022**, *51*, 6129–6147.
- [4] C. Yoo, Y. Lee, *Chem. Sci.* **2017**, *8*, 600–605.
- [5] a) D. W. Stephan, G. Erker, *Chem. Sci.* **2014**, *5*, 2625–2641; b) F.-G. Fontaine, M.-A. Courtemanche, M.-A. Légaré, E. Rochette, *Coord. Chem. Rev.* **2017**, *334*, 124–135.
- [6] a) Y. Jiang, O. Blacque, T. Fox, H. Berke, *J. Am. Chem. Soc.* **2013**, *135*, 7751–7760; b) S. J. K. Forrest, J. Clifton, N. Fey, P. G. Pringle, H. A. Sparkes, D. F. Wass, *Angew. Chem. Int. Ed.* **2015**, *54*, 2223–2227; *Angew. Chem.* **2015**, *127*, 2251–2255; c) Z. Jian, G. Kehr, C. G. Daniliuc, B. Wibbeling, T. Wiegand, M. Siedow, H. Eckert, M. Bursch, S. Grimme, G. Erker, *J. Am. Chem. Soc.* **2017**, *139*, 6474–6483; d) M. Devillard, R. Declercq, E. Nicolas, A. W. Ehlers, J. Backs, N. Saffon-Merceron, G. Bouhadir, J. C. Slootweg, W. Uhl, D. A. Bourissou, *J. Am. Chem. Soc.* **2016**, *138*, 4917–4926.
- [7] Y.-E. Kim, J. Kim, Y. Lee, *Chem. Commun.* **2014**, *50*, 11458–11461.
- [8] a) E. E. Benson, C. P. Kubiak, A. J. Sathrum, J. M. Smieja, *Chem. Soc. Rev.* **2009**, *38*, 89–99; b) O. Cooper, C. Camp, J. Pécaut, C. E. Kefalidis, L. Maron, S. Gambarelli, M., *J. Am. Chem. Soc.* **2014**, *136*, 6716–6723; c) J. A. Buss, D. G. VanderVelde, T. Agapie, *J. Am. Chem. Soc.* **2018**, *140*, 10121–10125.
- [9] a) R. C. Cammarota, M. V. Vollmer, J. Xie, J. Ye, J. C. Linehan, S. A. Burgess, A. M. Appel, L. Gagliardi, C. C. A. Lu, *J. Am. Chem. Soc.* **2017**, *139*, 14244–14250; b) J. Takaya, N. Iwasawa, *J. Am. Chem. Soc.* **2017**, *139*, 6074–6077; c) J. R. Prat, C. A. Gaggioli, R. C. Cammarota, E. Bill, L. Gagliardi, C. C. Lu, *Inorg. Chem.* **2020**, *59*, 14251–14262.
- [10] a) S. Bontemps, L. Vendier, S. Sabo-Etienne, *Angew. Chem. Int. Ed.* **2012**, *51*, 1671–1674; *Angew. Chem.* **2012**, *124*, 1703–1706; b) S. Bontemps, S. Sabo-Etienne, *Angew. Chem. Int. Ed.* **2013**, *52*, 10253–10255; *Angew. Chem.* **2013**, *125*, 10443–10445; c) G. Jin, C. G. Werncke, Y. Escudí, S. Sabo-Etienne, S. Bontemps, *J. Am. Chem. Soc.* **2015**, *137*, 9563–9566; d) S. Bontemps, *Coord. Chem. Rev.* **2016**, *308*, 117–130; e) M. D. Sampson, C. P. Kubiak, *J. Am. Chem. Soc.* **2016**, *138*, 1386–1393; f) M. Rauch, G. Parkin, *J. Am. Chem. Soc.* **2017**, *139*, 18162–18165; g) J. E. Heimann, W. H. Bernskoetter, N. Hazari, *J. Am. Chem. Soc.* **2019**, *141*, 10520–10529.
- [11] S. Sinhababu, M. R. Radzhabov, J. Tesler, N. P. Mankad, *J. Am. Chem. Soc.* **2022**, *144*, 3210–3221.
- [12] H.-Y. Liu, R. J. Schwamm, M. S. Hill, M. F. Mahon, C. L. McMullin, N. A. Rajabi, *Angew. Chem. Int. Ed.* **2021**, *60*, 14390–14393; *Angew. Chem.* **2021**, *133*, 14511–14514.
- [13] a) C. Weetman, P. Bag, T. Szilvási, C. Jandl, S. Inoue, *Angew. Chem. Int. Ed.* **2019**, *58*, 10961–10965; *Angew. Chem.* **2019**, *131*, 11077–11081; b) C. Weetman, A. Porzelt, P. Bag, F. Hanusch, S. Inoue, *Chem. Sci.* **2020**, *11*, 4817–4827; c) M. M. D. Roy, J. Hicks, P. Vasko, A. Heilmann, A.-M. Baston, J. M. Goicoechea, S. Aldridge, *Angew. Chem. Int. Ed.* **2021**, *60*, 22301–22306; *Angew. Chem.* **2021**, *133*, 22475–22480.
- [14] L. Escomel, I. Del Rosal, L. Maron, E. Jeanneau, L. Veyre, C. Thieuleux, C. Camp, *J. Am. Chem. Soc.* **2021**, *143*, 4844–4856.
- [15] a) J. Hicks, A. Mansikkamäki, P. Vasko, J. M. Goicoechea, S. A. Aldridge, *Nat. Chem.* **2019**, *11*, 237–241; b) C. McManus, J. Hicks, X. Cui, L. Zhao, G. Frenking, J. M. Goicoechea, S. Aldridge, *Chem. Sci.* **2021**, *12*, 13458–13468.
- [16] a) J. Campos, *J. Am. Chem. Soc.* **2017**, *139*, 2944–2947; b) N. Hidalgo, J. J. Moreno, M. Pérez-Jiménez, C. Maya, J. López-Serrano, J. Campos, *Chem. Eur. J.* **2020**, *26*, 5982–5993; c) M. G. Alférez, N. Hidalgo, J. J. Moreno, J. Campos, *Angew. Chem. Int. Ed.* **2020**, *59*, 20863–20867; *Angew. Chem.* **2020**, *132*, 21049–21053; d) M. Navarro, J. Campos, Chapter 3 in *Adv. Organomet. Chem.*, Vol. 75 (Ed.: Pedro J. Pérez), Elsevier, Amsterdam, **2021**.
- [17] a) M. Hirano, M. Akita, K. Tani, K. Kumagai, N. C. Kasuga, A. Fukuoka, S. Komiyama, *Organometallics* **1997**, *16*, 4206–4213; b) T. T. Adamson, S. P. Kelley, W. H. Bernskoetter, *Organometallics* **2020**, *39*, 3562–3571; c) P. M. Jurd, H. L. Li, M. Bhadrabade, L. D. Field, *Organometallics* **2020**, *39*, 2011–2018.
- [18] J. B. Geri, J. P. Shanahan, N. K. Szymczak, *J. Am. Chem. Soc.* **2017**, *139*, 5952–5956.
- [19] D. H. Gibson, M. Ye, B. A. Sleadd, J. M. Mehta, O. P. Mbadike, J. F. Richardson, M. S. Mashuta, *Organometallics* **1995**, *14*, 1242–1255.
- [20] a) T. Kaehler, R. L. Melen, *Cell Rep. Phys. Sci.* **2021**, *2*, 100595; b) A. Y. Timoshkin, G. Frenking, *Organometallics* **2008**, *27*, 371–380. See also: c) J. J. Cabrera-Trujillo, I. Fernández, *Chem. Eur. J.* **2018**, *24*, 17823–17831.
- [21] a) A. F. R. Kilpatrick, F. G. N. Cloke, *Chem. Commun.* **2014**, *50*, 2769–2771; b) A. Noor, S. Qayyum, T. Bauer, S. Schwarz, B. Weber, R. Kempe, *Chem. Commun.* **2014**, *50*, 13127–13130; c) C. T. Saouma, M. W. Day, J. C. Peters, *Chem. Sci.* **2013**, *4*, 4042–4051; d) R. Shimogawa, T. Takao, G. I. Konishi, H. Suzuki, *Organometallics* **2014**, *33*, 5066–5069; e) B. Bagherzadeh, N. P. Mankad, *Chem. Commun.* **2018**, *54*, 1097–1100.
- [22] J. P. Krogman, B. M. Foxman, C. M. Thomas, *J. Am. Chem. Soc.* **2011**, *133*, 14582–14585.
- [23] a) D. E. DeRossa, B. Q. Mercado, G. Lukat-Rodgers, K. R. Rodgers, P. L. Holland, *Angew. Chem. Int. Ed.* **2017**, *56*, 3211–3215; *Angew. Chem.* **2017**, *129*, 3259–3263; b) X. Engelmann, S. Yao, E. R. Farquhar, T. Szilvási, U. Kuhlmann, P. Hildebrandt,

- M. Driess, K. A. Ray, *Angew. Chem. Int. Ed.* **2017**, *56*, 297–301; *Angew. Chem.* **2017**, *129*, 303–307.
- [24] a) S. C. Davies, D. L. Hughes, R. L. Richards, J. R. Sanders, *Dalton Trans.* **2002**, 1442–1447; b) E. C. Weintrob, D. Tofan, J. E. Bercaw, *Inorg. Chem.* **2009**, *48*, 3808–3813; c) J. M. Becker, J. Barker, G. J. Clarkson, R. van Gorkum, G. K. Johal, R. I. Walton, P. Scott, *Dalton Trans.* **2010**, *39*, 2309–2326.
- [25] R. H. Crabtree, *The Organometallic Chemistry of the Transition Metals*, 7th ed., Wiley, Hoboken, **2019**.
- [26] a) M. Hirano, M. Akita, T. Morikita, H. Kubo, A. Fukuoka, S. Komiya, *J. Chem. Soc. Dalton Trans.* **1997**, 3453–3458; b) M. V. Baker, L. D. Field, *J. Am. Chem. Soc.* **1986**, *108*, 7436–7438.
- [27] a) A. Berkefeld, W. E. Piers, M. Parvez, L. Castro, L. Maron, O. Eisenstein, *Chem. Sci.* **2013**, *4*, 2152–2162; b) T. Wang, M. Xu, A. R. Jupp, Z.-W. Qu, S. Grimme, D. W. Stephan, *Angew. Chem. Int. Ed.* **2021**, *60*, 25771–25775; *Angew. Chem.* **2021**, *133*, 25975–25979; c) M. T. Bautista, P. Cappellani, S. D. Drouin, R. H. Morris, C. T. Schweitzer, A. Sella, J. Zubkowski, *J. Am. Chem. Soc.* **1991**, *113*, 4876–4887.
- [28] T. Voss, T. Mahdi, E. Otten, R. Fröhlich, G. Kehr, D. W. Stephan, G. Erker, *Organometallics* **2012**, *31*, 2367–2378.
- [29] a) G. M. Bancroft, M. J. Mays, B. E. Prater, F. P. Stefanini, *J. Chem. Soc. A* **1970**, 2146–2149; b) S. D. Drouin, P. A. Maltby, B. E. Rennie, C. T. Schweitzer, A. Golombek, P. Cappellani, R. H. Morris, *Inorg. Chim. Acta* **2021**, *516*, 120124.
- [30] M. F. Espada, J. Campos, J. López-Serrano, M. L. Poveda, E. Carmona, *Angew. Chem. Int. Ed.* **2015**, *54*, 15379–15384; *Angew. Chem.* **2015**, *127*, 15599–15604.
- [31] J. Bauer, H. Braunschweig, R. D. Dewhurst, *Chem. Rev.* **2012**, *112*, 4329–4346.
- [32] D. Specklin, A. Coffinet, L. Vendier, I. Del Rosal, C. Dinoi, A. Simonneau, *Inorg. Chem.* **2021**, *60*, 5545–5562.
- [33] S. Komiya, M. Akita, A. Yoza, N. Kasuga, A. Fukuoka, Y. Kai, *J. Chem. Soc. Chem. Commun.* **1993**, 787–788.
- [34] Additional calculations using [Fe]²⁺ and [Au]¹⁺ as fragments, which is consistent with the relative electronegativities of iron and gold, indicate that the [Fe]⁰/[Au]⁺ fragmentation better describes the bonding situation in complex **6**⁺ (see Supporting Information).
- [35] K. P. A. Kepp, *Inorg. Chem.* **2016**, *55*, 9461–9470.
- [36] a) N. Hidalgo, C. Romero-Pérez, C. Maya, I. Fernández, J. Campos, *Organometallics* **2021**, *40*, 1113–1119; b) A. L. Liberman-Martin, D. S. Levine, M. S. Ziegler, R. G. Bergman, T. D. Tilley, *Chem. Commun.* **2016**, *52*, 7039–7042.
- [37] Deposition Numbers 2172175, 2172176, 2172177, 2172178 and 2172179 contain the supplementary crystallographic data for this paper. These data are provided free of charge by the joint Cambridge Crystallographic Data Centre and Fachinformationszentrum Karlsruhe Access Structures service.

Manuscript received: May 23, 2022

Accepted manuscript online: August 5, 2022

Version of record online: August 29, 2022